



### **Science Arts & Métiers (SAM)**

is an open access repository that collects the work of Arts et Métiers Institute of Technology researchers and makes it freely available over the web where possible.

This is an author-deposited version published in: <https://sam.ensam.eu>  
Handle ID: <http://hdl.handle.net/10985/23273>

#### **To cite this version :**

Mohammad Saeid AGHIGHI, Amine AMMAR, Hamed MASOUMI, A. LANJABI - Rayleigh–Bénard convection of a viscoplastic liquid in a trapezoidal enclosure - International Journal of Mechanical Sciences - Vol. 180, p.105630 - 2020

Any correspondence concerning this service should be sent to the repository

Administrator : [scienceouverte@ensam.eu](mailto:scienceouverte@ensam.eu)



# Rayleigh–Bénard convection of a viscoplastic liquid in a trapezoidal enclosure

M.S. Aghighi<sup>a,\*</sup>, A. Ammar<sup>b</sup>, H. Masoumi<sup>a</sup>, A. Lanjani<sup>a</sup>

<sup>a</sup> Department of Mechanical Engineering, Bu-Ali Sina University, 65175-38695 Hamedan, Iran

<sup>b</sup> Arts et Métiers ParisTech, 2 Boulevard du Ronceray, BP 93525, F-49035 Angers cedex 01, France

## Keywords:

Rayleigh–Bénard

Yield stress

Bingham model

Trapezoidal enclosure

Finite element method

The objective of this paper is to clarify the role of sloping walls on convective heat transport in Rayleigh–Bénard convection within a trapezoidal enclosure filled with viscoplastic fluid. The rheology of the viscoplastic fluid has been modeled with Bingham fluid model. The system of coupled nonlinear differential equations was solved numerically by Galerkin's weighted residuals scheme of finite element method. The numerical experiments are carried out for a range of parameter values, namely, Rayleigh number ( $5.10^3 \leq Ra \leq 10^5$ ), yield number ( $0 \leq Y \leq Y_c$ ), and sidewall inclination angle ( $\phi = 0, \pi/6, \pi/4, \pi/3$ ) at a fixed Prandtl number ( $Pr = 500$ ). Effects of the inclination angle on the flow and temperature fields are presented. The results reveal that inclination angle causes a multicellular flow and appears as the main parameter to govern heat transfer in the cavity. The heat transfer rate is found to increase with the increasing angle of the sloping wall for both Newtonian and yield stress fluids. On the other hand, the plug regions also found to increase with increasing  $\phi$ , which is unusual but perhaps not unexpected behavior. In the yield stress fluids, the flow becomes motionless above a critical yield number  $Y_c$  because the plug regions invade the whole cavity. The critical yield number  $Y_c$  is also affected by the change of inclination angle and increases significantly with the increase of  $\phi$ .

## 1. Introduction

Rayleigh–Bénard convection is a type of natural convection where fluid motion is driven by vertical thermal gradients, i.e., by buoyancy forces. This problem has been studied by many researchers during the past several decades owing to their wide applications in a number of industrial processes, such as heat exchangers, electronic cooling, solar collectors, etc. Over this period, numerous studies related to Newtonian fluids have been documented in the literature, e.g., see the extensive studies of Bodenschatz et al. [1]. A subsequent more detailed study has been done by Ouertatani et al. [2] where the steady-state condition of two-dimensional Rayleigh–Bénard convection was analyzed numerically by using the finite volume method. There are also some experimental works such as Maystrenko et al. [3] research about measurements of the temperature distribution in the upper (cold) boundary layer of a rectangular Rayleigh–Bénard cell. The problems related to Rayleigh–Bénard convection in porous media, nanofluids and non-Newtonian power-law fluids have been considered by several researchers in the last years and a good amount of work can be found in the literature. The interested reader is referred to [4–8] for more complete coverage.

Rayleigh–Bénard convection of viscoplastic fluids has also received extensive attention in the past decades. However, most of the research

works in this field are substantially oriented toward the study of rectangular enclosures. The effects of a fluid yield stress on the classical Rayleigh–Bénard instability in the cavity have been investigated by Zhang et al. [9] and Vikhansky [10]. Turan et al. [11] analyzed the effect of yield stress on laminar Rayleigh–Bénard convection in a square enclosure filled with a Bingham fluid and showed that the value of heat transfer decreases with increasing yield stress. It means that yield stress has a stabilizing effect, reducing the convection intensity. Study of Rayleigh–Bénard convection of viscoplastic material extended to the Herschel–Bulkley fluids by Hassan et al. [12] and Aghighi and Ammar [13]. Recently, Rayleigh–Bénard convection of viscoplastic fluids obeying the Casson model has been investigated by Aghighi et al. [14]. Many more studies related to the natural convection of viscoplastic fluids can be found in the literature. The interested reader is referred to [15–18] for more complete coverage.

Natural convection of fluid contained in a trapezoidal enclosure is one of the most extensively analyzed configurations because of its applicability in various fields such as ventilation of building, electronic cooling, geothermal problems, solar energy collector, etc. Whereas there exists an overwhelming number of fundamentally important studies of the natural convection within trapezoidal enclosure in Newtonian and power-law fluids, to the best of our knowledge, there is no research deal-

\* Corresponding author.

E-mail addresses: [ms.aghighi@basu.ac.ir](mailto:ms.aghighi@basu.ac.ir) (M.S. Aghighi), [amine.ammar@ensam.eu](mailto:amine.ammar@ensam.eu) (A. Ammar).

## Nomenclature

$Bn$	Bingham number ( $\equiv (Pr/Ra)^{-1/2} \frac{\tau_y}{\rho\beta g\Delta TH}$ )
$C_p$	specific heat capacity, $\text{kJ kg}^{-1} \text{K}^{-1}$
$g$	acceleration due to gravity, $\text{m s}^{-2}$
$H$	reference value of length, $m$
$k$	thermal conductivity, $\text{W m}^{-1} \text{K}^{-1}$
$L$	length of the cavity, dimensionless
$m$	Papanastasiou regularization parameter, dimensionless
$Nu$	local Nusselt number, dimensionless
$\overline{Nu}$	average Nusselt number, dimensionless
$n_s$	outward unit normal vector to the sidewall, dimensionless
$p$	pressure, dimensionless
$p_0$	reference value of pressure, Pa
$Pr$	Prandtl number ( $\equiv \mu/\rho\alpha$ ), dimensionless
$Ra$	Rayleigh number ( $\equiv \frac{\rho\beta g\Delta TH^3}{\mu\alpha}$ ), dimensionless
$T$	temperature of fluid, K
$T_r$	reference temperature, K
$u$	velocity component in $x$ direction, dimensionless
$u_0$	reference velocity, $\text{m s}^{-1}$
$v$	velocity component in $y$ direction, dimensionless
$x, y$	Cartesian coordinates, dimensionless
$Y$	yield number ( $\equiv \frac{\tau_y}{\rho\beta g\Delta TH}$ ), dimensionless
$Y_c$	critical yield number, dimensionless

## Greek symbols

$\alpha$	thermal diffusivity of fluid, $\text{m}^2 \text{s}^{-1}$
$\beta$	coefficient of thermal expansion, $\text{K}^{-1}$
$\dot{\gamma}$	rate of strain tensor, dimensionless
$\theta$	temperature, dimensionless
$\nu$	kinematic viscosity, $\text{m}^2 \text{s}^{-1}$
$\lambda$	penalty parameter, dimensionless
$\mu$	plastic viscosity, Pa s
$\rho$	density of fluid, $\text{kg m}^{-3}$
$\tau$	stress tensor, dimensionless
$\tau_y$	yield stress of fluid, dimensionless
$\varphi$	side wall inclination angle

## Subscripts

$b$	bottom
$C$	cold
$H$	hot
$m$	mid
$p$	pervious
$t$	top

ing with this problem in viscoplastic liquid. One of the first numerical and experimental works about the natural convection of Newtonian fluids in a trapezoidal enclosure has been done by Lee [19]. After that, Karyakin [20] analyzed the transient natural convection of Newtonian fluids in this geometry by using the implicit finite-difference method. Their studies showed that the heat transfer rate increased as the angle of the side wall increased. Natural convection of Newtonian fluid in a trapezoidal cavity heated from below has been investigated by Basak et al. [21] using finite element method. This problem extended to porous materials by Varol et al. [22]. One of the first investigations related to natural convection of nanofluids in a trapezoidal cavity was performed by Saleh et al. [23]. A more detailed study about the effect of nanoparticles on natural convection heat transfer in this geometry has been done by Al-Weheibi et al. [24]. In the recent years a number of investigations have been conducted to obtain an understanding of the behavior of the more complex fluid flows in this geometry. Gibano et al. [25] and Miroshnichenko et al. [26] analyzed natural convection

of a micropolar fluid in a trapezoidal cavity. Convective heat transfer in trapezoidal cavity with nonuniformly heated bottom wall under the influence of magnetic field was investigated by Hossain and Alim [27] and MHD natural convection of ferrofluid in an open trapezoidal cavity filled with a porous medium was studied by Astanina et al. [28]. Entropy generation on natural convection has also been scrutinized in this study. After that, Al-Sayegh [29] extended the previous problem to three-dimensional flow patterns of nanofluids. A numerical analysis of convective heat transfer for non-Newtonian (power-law) nanofluid was reported by Alsabery et al. [30]. Recently, Al-Mudhaf et al. [31] investigated the Soret and Dufour effects on the unsteady double-diffusive natural convection inside trapezoidal enclosures filled with isotropic porous medium.

On the basis of literature reviewed as above, it can be concluded that despite a large number of numerical studies on natural convection within a trapezoidal cavity, which have been reported in the literature, there is a serious lack of information regarding the problem of fluid flow and heat transfer enhancement of viscoplastic materials in this geometry. Therefore, the aim of the present investigation is to study the effect of sloping wall on Rayleigh-Bénard convection of a viscoplastic fluid in a trapezoidal cavity.

## 2. Mathematical formulation

The system considered in this study is a trapezoidal cavity of height  $H$  with the side wall inclined at an angle  $\varphi = 0, \pi/6, \pi/4, \pi/3$  with  $y$  axis. The schematic diagram of the physical model and coordinate system is given in Fig. 1. The cavity is filled with a yield stress fluid obeying the Bingham model. The bottom wall is heated isothermally with temperature  $T_h$  and the top wall is cooled isothermally with temperature  $T_c$  and the remaining sloping walls are considered adiabatic. Thermo-physical properties of the fluid are assumed to be constant except for the density variation, which is determined based on the Boussinesq approximation. Basis of the assumptions mentioned above and using the characteristic scales  $H$  for length,  $u_0 = (g\beta H\Delta T)^{1/2}$  for the velocity and  $p_0 = (\rho u_0^2)$  for the pressure, the governing equations describing the Rayleigh-

Bénard convection of viscoplastic fluid in their nondimensionalized form can be written as:

$$\begin{aligned} \frac{\partial u}{\partial x} + \frac{\partial v}{\partial y} &= 0 \\ u \frac{\partial u}{\partial x} + v \frac{\partial u}{\partial y} &= -\frac{\partial p}{\partial x} + Pr^{\frac{1}{2}} Ra^{\frac{-1}{2}} \left( \frac{\partial \tau_{xx}}{\partial x} + \frac{\partial \tau_{yx}}{\partial y} \right) \\ u \frac{\partial v}{\partial x} + v \frac{\partial v}{\partial y} &= -\frac{\partial p}{\partial y} + Pr^{\frac{1}{2}} Ra^{\frac{-1}{2}} \left( \frac{\partial \tau_{xy}}{\partial x} + \frac{\partial \tau_{yy}}{\partial y} \right) + \theta \\ u \frac{\partial \theta}{\partial x} + v \frac{\partial \theta}{\partial y} &= (Ra.Pr)^{\frac{-1}{2}} \left( \frac{\partial^2 \theta}{\partial x^2} + \frac{\partial^2 \theta}{\partial y^2} \right) \end{aligned} \quad (1)$$

Where  $u, v, \theta$ , and  $p$  are dimensionless horizontal velocity, vertical velocity, temperature, and pressure respectively.

The relevant boundary conditions of velocity are considered as no-slip on solid boundaries:

$$u = v = 0 \text{ on all walls.} \quad (2)$$

Adiabatic conditions are written at side walls and imposed temperatures at horizontal walls:

$$\begin{aligned} \frac{\partial \theta}{\partial n_s} &= 0 \text{ at side walls} \\ \theta &= 0.5 \text{ at } y = 0 \\ \theta &= -0.5 \text{ at } y = 1 \end{aligned} \quad (3)$$

where  $n_s$  is the outward unit normal vector to the sidewall.

The dimensionless temperature  $\theta$  is defined by:

$$\theta = \frac{T - T_r}{T_H - T_C} \quad (4)$$

where  $T_r$  is a reference temperature:  $T_r = (T_H + T_C)/2$ .

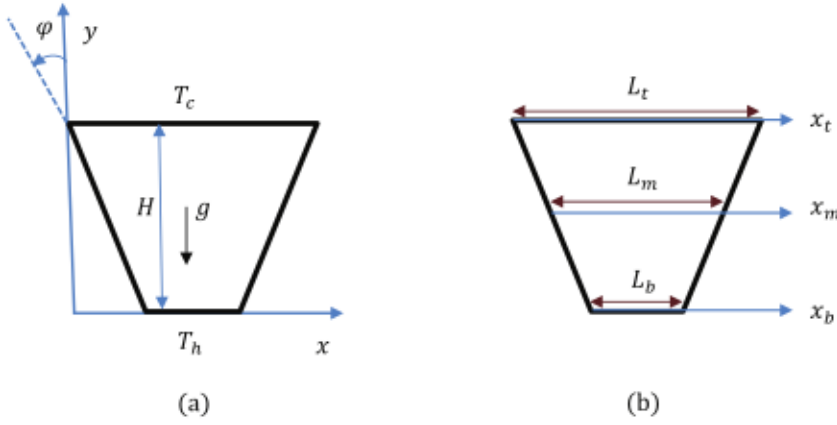


**Fig. 1.** Schematic diagram of the physical model and coordinate system.  $(x, y)$ : main coordinate system,  $x_b$ : x-coordinate along the bottom wall,  $x_m$ : x-coordinate along the horizontal mid-plane,  $x_t$ : x-coordinate along the top wall.

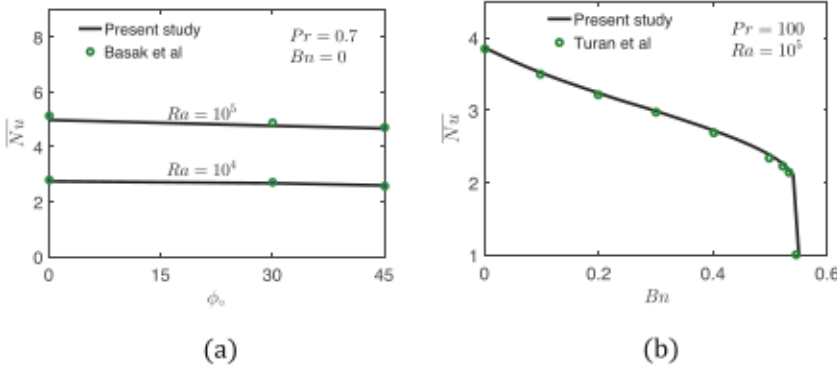


**Fig. 2.** (a): Validation of the present code results for mean Nusselt number  $\overline{Nu}$  of Newtonian fluids in a trapezoidal cavity (present study and Basak study [21]) and (b): Validation of the present code results for mean Nusselt number  $\overline{Nu}$  of Bingham fluids in a square enclosure (present study and Turan study [11]).

The stress-deformation behavior of viscoplastic materials based on Bingham model is given by:

$$\tau_{ij} = \left(1 + \left(\frac{Bn}{\dot{\gamma}}\right)\right) \dot{\gamma}_{ij} \text{ for } |\tau| > \tau_y \text{ and } \dot{\gamma} = 0 \text{ for } |\tau| < \tau_y \quad (5)$$

For  $i, j = 1, 2$  with  $(x_1, x_2) = (x, y)$ , where  $\tau$  is the viscous stress,  $Bn$  is Bingham number,  $\dot{\gamma} = \sqrt{\frac{1}{2} \dot{\gamma}_{ij} \dot{\gamma}_{ij}}$  and  $\tau = \sqrt{\frac{1}{2} \tau_{ij} \tau_{ij}}$ .

The rate-of-strain tensor  $\dot{\gamma}_{ij}$  is defined by:

$$\dot{\gamma}_{ij} = \frac{\partial u_i}{\partial x_j} + \frac{\partial u_j}{\partial x_i} \quad (6)$$

The Prandtl number,  $Pr$ , Rayleigh number,  $Ra$ , and Bingham number,  $Bn$ , defined by:

$$Pr = \frac{\mu C_p}{k}, \quad Ra = \frac{g \beta \Delta T H^3}{\alpha \nu}, \quad Bn = \left(\frac{Pr}{Ra}\right)^{-1/2} \frac{\tau_y}{\rho \beta g \Delta T H} = \left(\frac{Pr}{Ra}\right)^{-1/2} Y \quad (7)$$

with  $Y$  the yield number which corresponds to the ratio between the yield stress and the buoyancy effects  $Y = \frac{\tau_y}{\rho \beta g \Delta T H}$ . It is worth noting that the yield number  $Y$  does not depend on  $Ra$  and  $Pr$  contrary to  $Bn$ .

The various dimensional quantities above are defined as follows:  $\mu$  is the dynamic viscosity,  $C_p$  is specific heat capacity,  $k$  is the thermal conductivity,  $g$  is the acceleration due to gravity,  $\beta$  is the coefficient of thermal expansion,  $\alpha$  is the thermal diffusivity,  $\Delta T$  is the temperature difference between hot and cold walls, and  $\nu$  is the kinematic viscosity.

As one can see, there is a discontinuity between yielded and unyielded regions since the stress tensor is indeterminate when  $|\tau| < \tau_y$  and the viscosity tends to infinity when  $\dot{\gamma} \rightarrow 0$ . To circumvent this difficulty, the Papanastasiou regularization of the constitutive equation is employed [32]. Based on this regularization, Eq. (5) can be rewritten as

follows:

$$\tau_{ij} = \left(1 + \left(\frac{Bn}{\dot{\gamma}}\right)(1 - \exp(-m\dot{\gamma}))\right) \dot{\gamma}_{ij} \quad (8)$$

where  $m$  is regularization parameter and controls the exponential rise in the stress at low rates of strain.

The heat flux averaged over the hot and cold walls is defined via the Nusselt number:

$$\overline{Nu} = -\int_0^1 \frac{\partial \theta}{\partial y} \Big|_{y=0,1} dx \quad (9)$$

### 3. Numerical analysis

#### 3.1. Method of solution

The set of coupled partial differential equations and boundary conditions described in the previous section are solved by an iterative algorithm implemented in house under MATLAB and based on the Galerkin weighted residual method of finite element formulation [33]. The nonuniform unstructured triangular elements are considered to fill the entire domain. The advantages of unstructured meshing are manifold, the main being that it gives a more accurate solution of the governing equations in the vicinity of the walls.

The numerical method described in [14] has been used to solve the system of nonlinear coupled partial differential equations (Eq. (1)). The advantages posed by such an approach are accuracy, stability and simulation performances (CPU time) which makes it suitable for analyzing coupled non-linear systems in different configurations by using both structured [13,14] and unstructured [17,18] grids. Based on this way, to solve the nonlinear system of equations (Eq. (1)), a penalty formulation of the incompressibility constraint has been considered [33]. So,



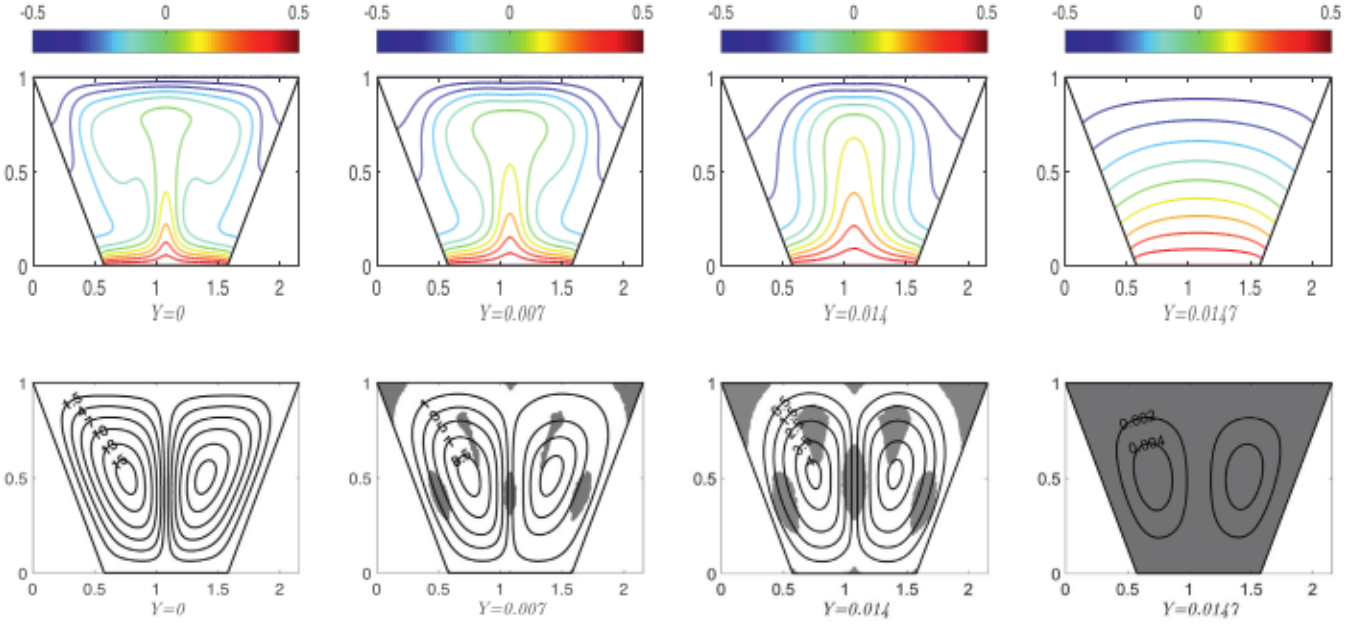


**Fig. 3.** Contours of non-dimensional temperature  $\theta$  (at the top) and stream functions with unyielded plug regions (at the bottom) for different values of yield number at  $Ra = 5.10^4$  and  $\varphi = \pi/6$ .

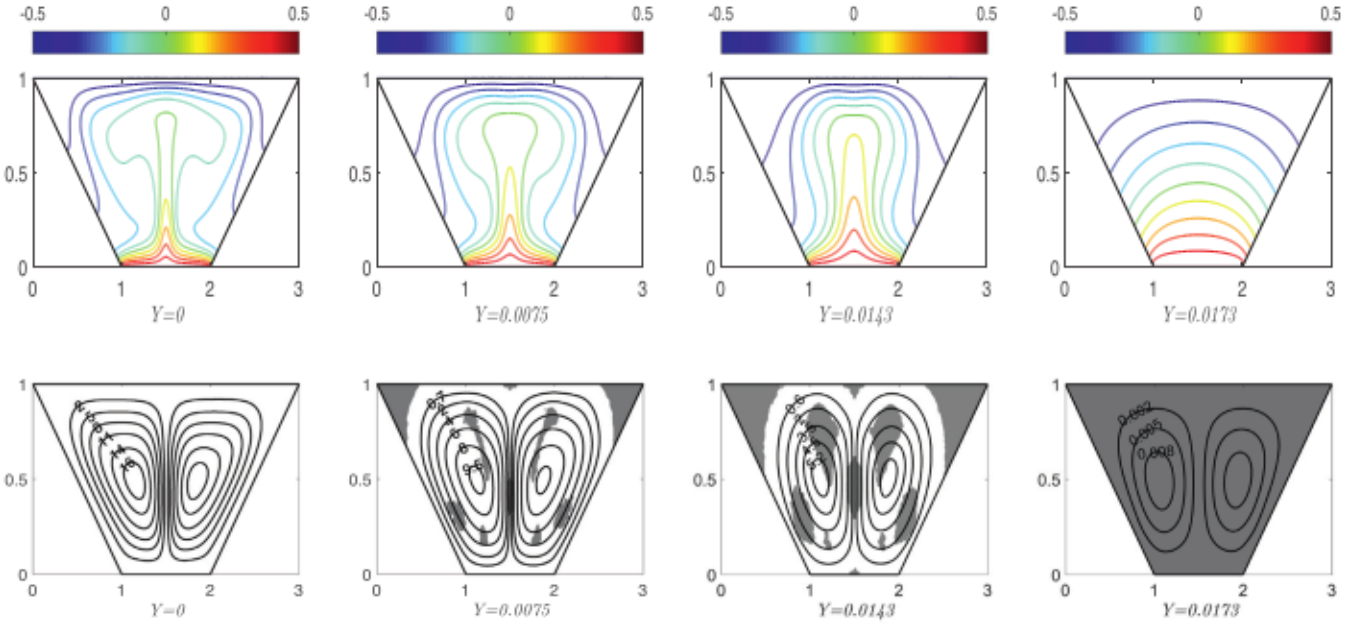


**Fig. 4.** Contours of non-dimensional temperature  $\theta$  (at the top) and stream functions with unyielded plug regions (at the bottom) for different values of yield number at  $Ra = 5.10^4$  and  $\varphi = \pi/4$ .

the governing equations will be rewritten in the following form:

$$\begin{aligned} \frac{\partial u}{\partial x} + \frac{\partial v}{\partial y} - \frac{p}{\lambda} &= 0 \\ u_p \frac{\partial u}{\partial x} + v_p \frac{\partial u}{\partial y} + \frac{\partial p}{\partial x} &= Pr^{\frac{1}{2}} Ra^{\frac{-1}{2}} \left( \frac{\partial \tau_{xx}}{\partial x} + \frac{\partial \tau_{yx}}{\partial y} \right)_p \\ u_p \frac{\partial v}{\partial x} + v_p \frac{\partial v}{\partial y} + \frac{\partial p}{\partial y} - \theta &= Pr^{\frac{1}{2}} Ra^{\frac{-1}{2}} \left( \frac{\partial \tau_{xy}}{\partial x} + \frac{\partial \tau_{yy}}{\partial y} \right)_p \\ u_p \frac{\partial \theta}{\partial x} + v_p \frac{\partial \theta}{\partial y} - (Ra \cdot Pr)^{\frac{-1}{2}} \left( \frac{\partial^2 \theta}{\partial x^2} + \frac{\partial^2 \theta}{\partial y^2} \right) &= 0 \end{aligned} \quad (10)$$

where  $\lambda$  is a large enough constant. In these equations, the subscript  $p$  denotes previous (initial) values of velocity and stress (the stress can also be computed based on  $u_p$  and  $v_p$ ). The velocity distribution of Newtonian fluids can be considered as the initial values of  $u_p$  and  $v_p$ . Based on

this way, previous (initial) values of velocity are imposed in the nonlinear convective terms, then the shear rate and shear stress are evaluated. From the momentum and energy equations, new values of velocity and temperature can be computed. These steps are repeated until the convergence of velocity and temperature fields. Further details of the method can be found in [14].

### 3.2. Numerical method validation

In order to assess the validity of the developed code, grid independent tests were conducted for both Newtonian and Bingham fluids ( $Ra = 10^5$  and  $0 \leq Bn \leq Bn_{max}$ ) and based on the results of velocity and

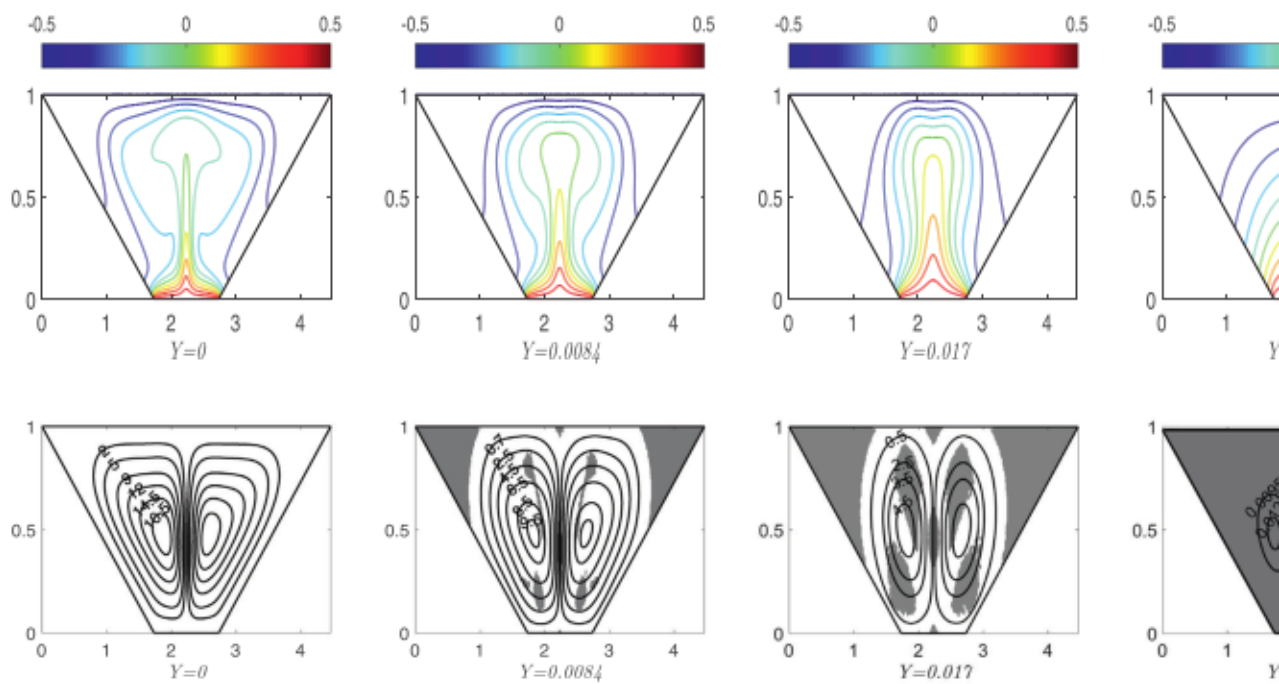
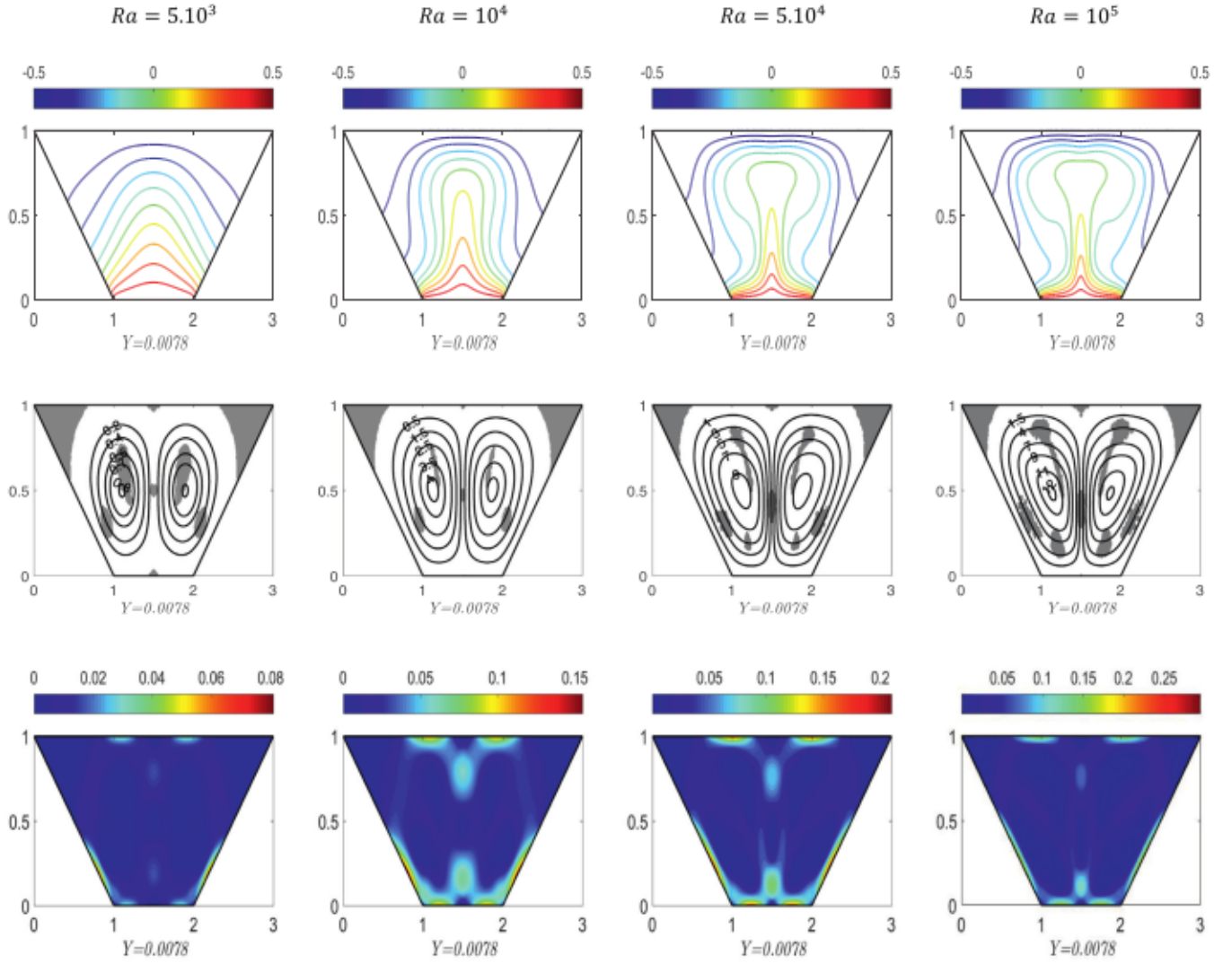


Fig. 5. Contours of non-dimensional temperature  $\theta$  (at the top) and stream functions with unyielded plug regions (at the bottom) for different values of yield number  $Y$ .



**Fig. 6.** Contours of non-dimensional temperature  $\theta$  (at the top), stream function with unyielded plug regions (in the middle) and the shear rate  $\dot{\gamma}$  (at the bottom) for different values of Rayleigh number at  $\varphi = \pi/4$  and  $Y = 0.0078$ .

heat transfer it was found that the mesh consisting of 7003 nodes guarantees a grid independent solution within the relative tolerance level of  $10^{-4}$ . The convergence of the solutions was also checked by varying the regularization ( $m$ ) and penalty ( $\lambda$ ) parameters defined in Eq. (8) and Eq. (10), respectively. It is found that the  $\overline{Nu}$  value converges within 0.1% by varying  $m$  and  $\lambda$  from  $10^3$  to  $10^4$ . Hence, in this study, both the regularization and penalty parameters are chosen to be  $10^4$ .

On the other hand, the numerical code was validated against the results of other numerical studies for natural convection in a cavity. Among them, natural convection of Newtonian fluid in a trapezoidal enclosure which compared with the similar study done by Basak [21]. Fig. 2(a) shows the comparison of mean Nusselt number  $\overline{Nu}$  with those results reported by Basak for different values of  $Ra$  at  $Pr = 0.7$ . The code is also verified with Rayleigh-Bénard convection of Bingham fluids in a square enclosure that is done by Turan [11] and very good accordance is obtained (Fig. 2(b)).

#### 4. Results and discussion

Numerical study has been conducted at the following values of the governing parameters: side wall angle ( $\varphi = 0, \pi/6, \pi/4, \pi/3$ ), yield number ( $0 \leq Y \leq Y_c$ ), and Rayleigh number ( $5.10^3 \leq Ra \leq 10^5$ ) at a constant value of the Prandtl number ( $Pr = 500$ ). The effects of these

parameters on heat and momentum transport have been discussed in detail.

##### 4.1. Streamlines and isotherm contours

Figs. 3–5 show the effects of side wall angle ( $\varphi = 0, \pi/6, \pi/4, \pi/3$ ) and yield number ( $0 \leq Y \leq Y_c$ ) on streamlines and isotherm contours at  $Ra = 5.10^4$  and  $Pr = 500$ . As one can see, the main feature of trapezoidal geometry is that the prevalent convective flow structure consists of two convection rolls while in a square cavity ( $\varphi = 0$ ) there is only one convection roll. This is due to the fact that with an increase in angle of inclined walls the length of the top cold wall increases compared to the bottom hot wall. As a result, warm fluid rises near the middle of the bottom wall towards the top wall and cold fluid descends near the side walls. Therefore, two symmetric rolls with clockwise and anti-clockwise rotations are formed in the right and left sides of the cavity, respectively. On the other hand, due to the significant convection force, the temperature contour lines start getting deformed and pushed towards the top wall and then shifted downward along the side walls.

The results obtained from different side wall angles ( $\varphi$ ) show that the thermal gradient near the walls increases with increasing  $\varphi$  and hence plume region extends and the values of stream functions increase. In these figures, the gray shades represent the unyielded (plug) regions.



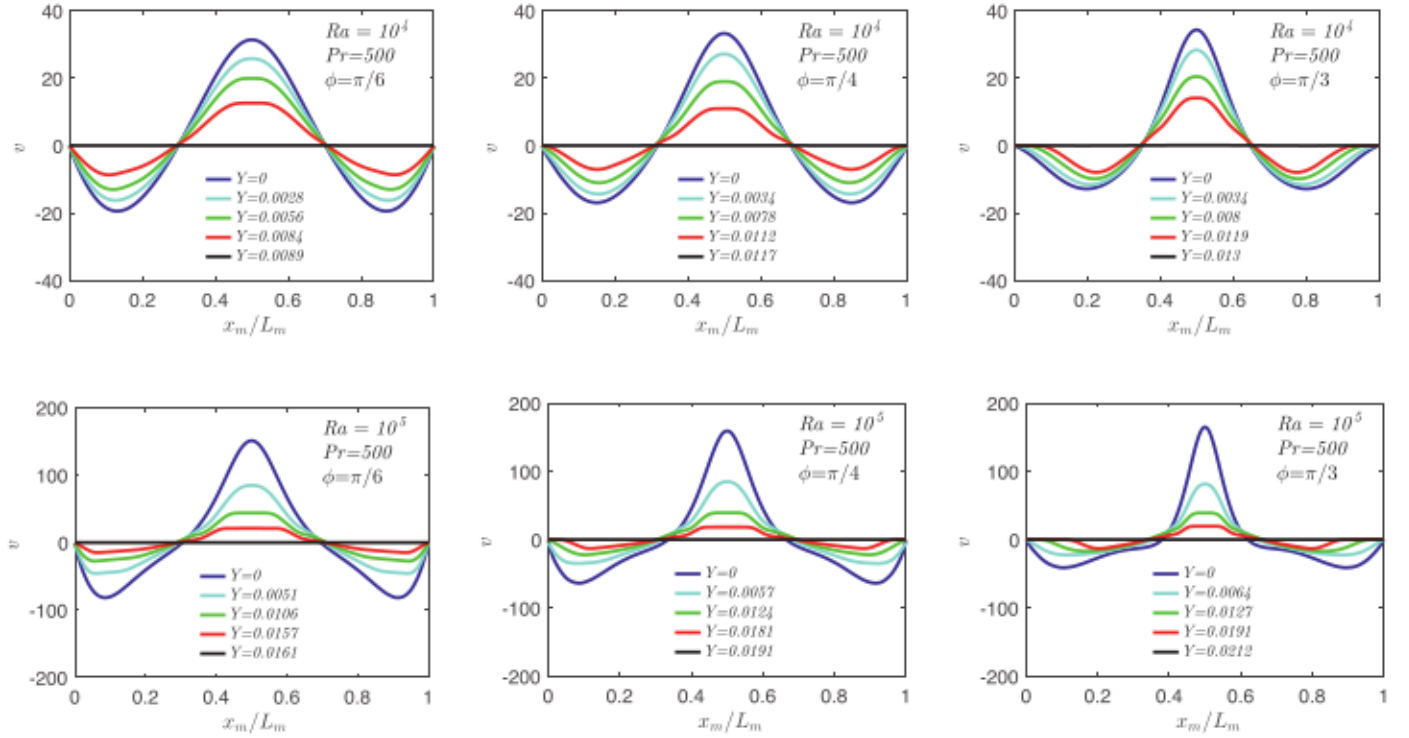


Fig. 7. Variations of non-dimensional velocity  $v$  with yield number  $Y$  along the horizontal mid-plane ( $y = 0.5$ ) for different values of sidewall inclination angle ( $\phi = \pi/6, \pi/4, \pi/3$ ) at  $Ra = 10^4$ (top) and  $Ra = 10^5$ (bottom).

Two types of plug regions can be observed in the region: The Truly Unyielded Regions (TUR) and the Apparently Unyielded Regions (AUR) [34]. The Truly Unyielded Regions (TUR) move with a plug velocity profile (no deformation). The Apparently Unyielded Regions (AUR) are located in the corners of the cavity and also in the zone of the stagnation points (middle of the horizontal walls). The unyielded plugs tend to accumulate at the top corners (acute angles) of the cavity where the velocities are very small and no deformation occurs. Comparing the unyielded region between the present trapezoidal geometry and square cavity ( $\phi = 0$ ) [11] shows that AUR in trapezoidal enclosure occupy more space in spite of the fact that the convective thermal transport strengthens. In other words, the heat transfer rate increases with increasing  $\phi$  due to the larger cold wall length and the plug regions increase with increasing  $\phi$  because of acute angle corners. It is interesting to note that in other geometries when the heat transfer rate increased the plug regions generally decreased.

Results show that the isotherm lines become smoother and plug regions increase with increasing  $Y$  because of stronger viscosity effects. In other words, by moving from  $Y = 0$  toward  $Y = Y_c$ , reduction in the isotherm's density near the horizontal walls decreases the heat transfer rate in viscoplastic fluids. It is observed that increasing the yield stress ( $Y$ ) decreases the magnitude of stream function, which confirms the stabilizing effect of the yield stress. As a result, plug regions increase with increasing  $Y$  and eventually, those inside the Apparently Unyielded Regions (AUR) are joined together with those in the convective area (TUR), forming a solid plug for high  $Y$  values.

The effects of  $Ra$  on streamline and isotherm contours for the fixed side wall inclination angle ( $\phi = \pi/4$ ) and yield number ( $Y = 0.0078$ ) are presented in Fig. 6. It is observed that as  $Ra$  increases, the isotherms become closer to the hot surface and the thermal gradient increases that leads to higher heat transfer rates. Also, the magnitude of stream functions increases by increasing  $Ra$  due to the strengthening of convective transport in the enclosure. However, a closer look at the results reveals that contrary to expectation, the unyielded regions increase with increasing  $Ra$  (except for  $Ra = 5 \cdot 10^3$ ). In order to explain this behavior,

the distribution of the second invariant of the shear rate tensor is also represented in this figure. The dark blue regions in this figure correspond to values of  $\dot{\gamma}$  which converge to zero, leading to unyielded regions. As expected, larger Rayleigh numbers lead to larger  $\dot{\gamma}$  values in the cavity but, in some areas the values of shear rate can even be reduced. In other words, an increase in  $Ra$  gives rise to strengthening of convection and hence plume region extends. As a result, the Apparently Unyielded Regions (AUR) decrease monotonically as  $Ra$  increases, but on the contrary, the Truly Unyielded Regions (TUR) start to increase at the domain because more space is available for them. However, it is worth to note that at low Rayleigh numbers ( $Ra < 10^4$ ), the unyielded regions (both AUR and TUR) increase due to weak convection current.

This behavior is in contrast to what is observed for the Rayleigh-Bénard convection of yield stress fluids in the square cavity.

#### 4.2. Velocity and temperature

Variations of non-dimensional vertical component of velocity  $v$  with  $Y$  along the horizontal mid-plane ( $y = 0.5$ ) of the cavity for  $Ra = 10^4, 10^5$  and  $\phi = 0, \pi/6, \pi/4, \pi/3$  are depicted in Fig. 7. The variations of temperature profile for the same conditions and configurations are represented in Fig. 8. As mentioned before, due to the hot bottom wall and cold top wall, warm fluid rises near the center of the cavity and cold fluid descends near the sloping walls. Existence of maximum and minimum points in velocity and temperature profiles is in accordance with the behavior observed in Figs 3-6. While the effect of side wall inclination angle  $\phi$  is seen to be weak at the center of cavity, it exerts much more influence on velocity and temperature profiles near the side walls. One can see that the temperature decreases in this area with the increase of  $\phi$  due to the effect of wider top cold wall. The results show that despite the fact that the strength of the convection currents increases with  $\phi$ , the vertical velocity profile decreases. This is due to the effect of side wall inclination angle  $\phi$  on the streamline patterns. In other words, sloping wall decreases the absolute magnitude of vertical velocity but increases the absolute magnitude of horizontal velocity.



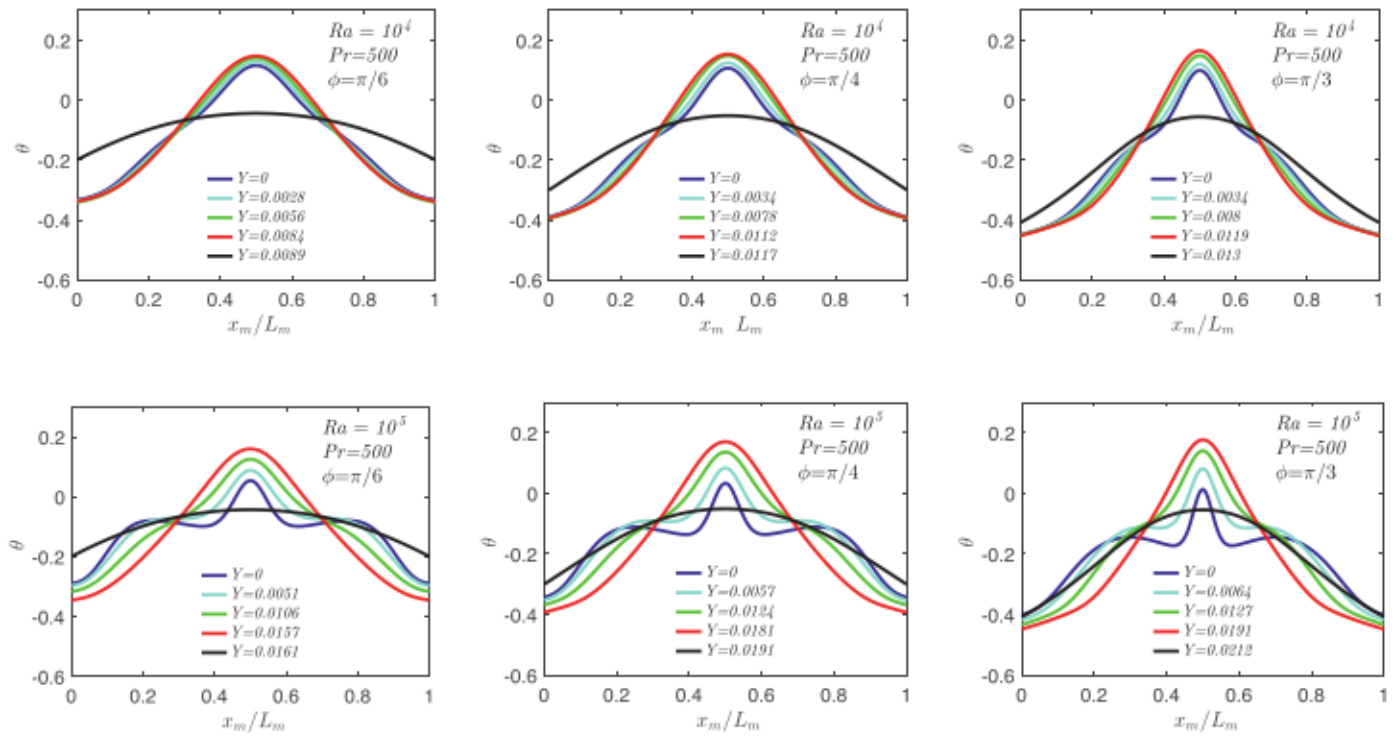


**Fig. 8.** Variations of non-dimensional temperature  $\theta$  with yield number  $Y$  along the horizontal mid-plane ( $y = 0.5$ ) for different values of sidewall inclination angle ( $\phi = \pi/6, \pi/4, \pi/3$ ) at  $Ra = 10^4$ (top) and  $Ra = 10^5$ (bottom).

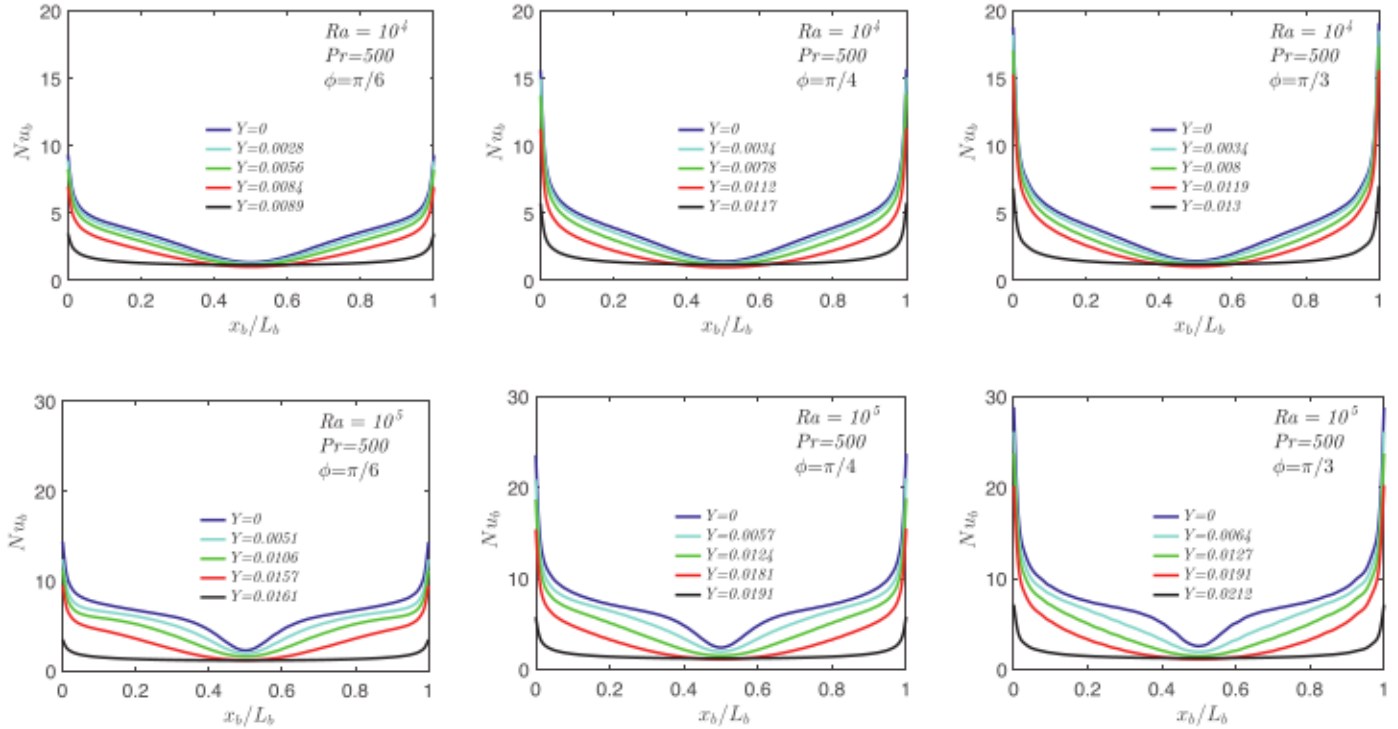


**Fig. 9.** Variations of local Nusselt number (along the bottom hot wall  $Nu_b$ ) with yield number  $Y$  for different values of sidewall inclination angle ( $\phi = \pi/6, \pi/4, \pi/3$ ) at  $Ra = 10^4$ (top) and  $Ra = 10^5$ (bottom).

Results show that, as  $Ra$  increases, the magnitude of velocity increases and temperature distribution becomes fairly non-linear due to stronger convection force. On the other hand, opposite trends are observed when the yield number increases which causes the fluid flow to decelerate and the strength of convection to reduce,

hence flow leads to an almost motionless conductive regime. Results show that the value of  $Y_c$  (yield number of the rest state) increases with increasing  $\phi$  and/or  $Ra$  due to the stronger buoyancy effects, which can overcome the flow resistance up to greater values of yield number.

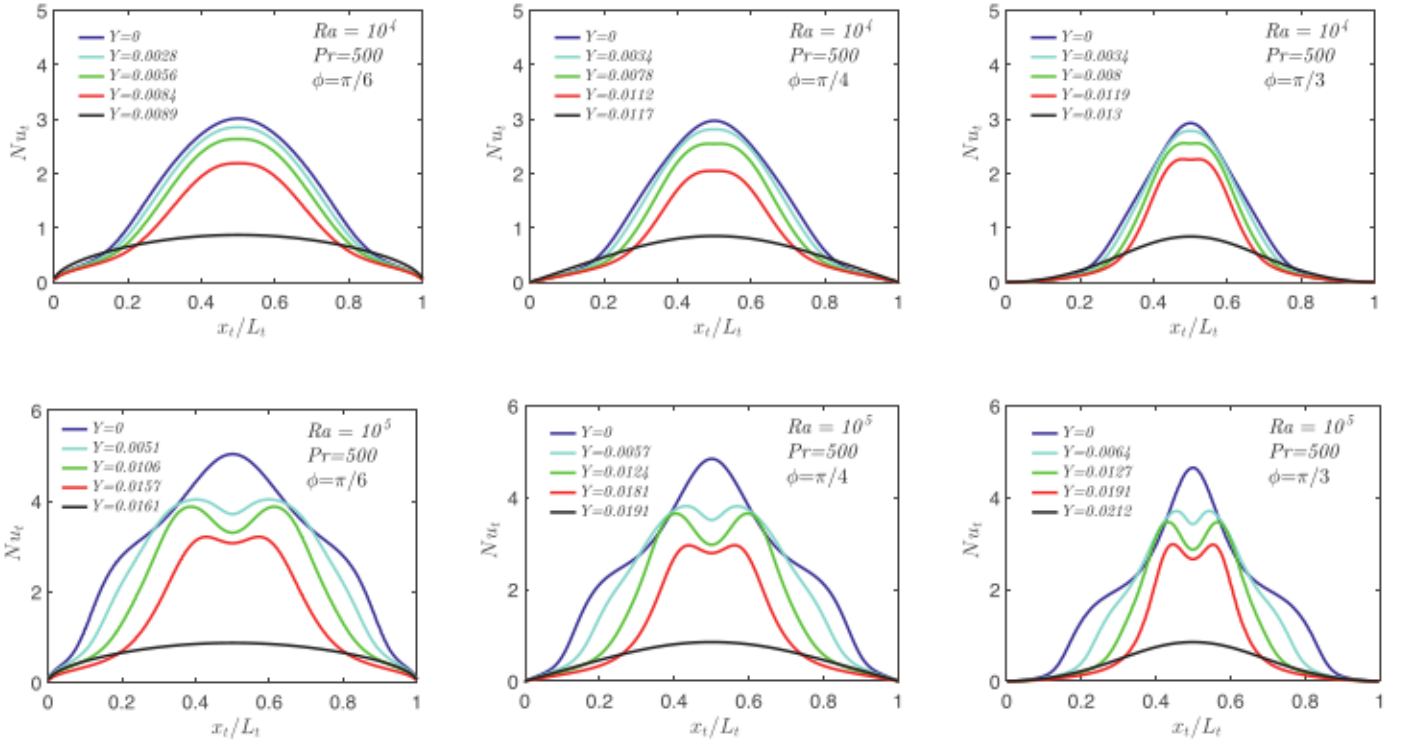


Fig. 10. Variations of local Nusselt number (along the top cold wall  $Nu_t$ ) with yield number  $Y$  for different values of sidewall inclination angle ( $\phi = \pi/6, \pi/4, \pi/3$ ) at  $Ra = 10^4$ (top) and  $Ra = 10^5$ (bottom).

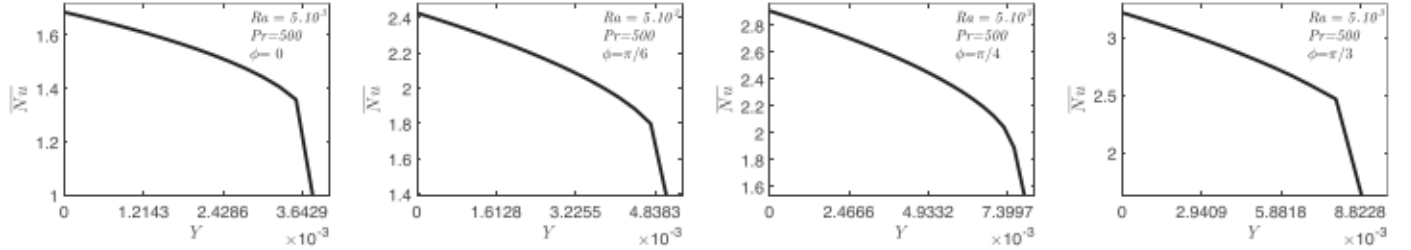


Fig. 11. Variations of mean Nusselt number  $\overline{Nu}$  with yield number  $Y$  along the hot bottom wall for different values of sidewall inclination angle ( $\phi = 0, \pi/6, \pi/4, \pi/3$ ) at  $Ra = 5.10^3$ .

#### 4.3. Local heat transfer

The effects of side wall inclination angle  $\phi$ , yield number  $Y$ , and Rayleigh number  $Ra$  on the local heat transfer at the bottom hot wall  $Nu_b$  have been presented in Fig. 9. Variations of local heat transfer rates at the top cold wall  $Nu_t$  for the same conditions and configurations are represented in Fig. 10. Fig. 9 shows that the local Nusselt number is maximum at the bottom corner of side walls where the temperature gradients are largest. Then it progressively decreases from its maximum value all the way to the mid-width ( $L_b = 0.5$ ) where there is no flow at the lower stagnation point. On the contrary, the Nusselt number is seen to be maximum at the central region of the top wall in the zone of the upper stagnation point where the hot fluid approaches the top cold wall and hence the isotherms are closely packed, whilst the heat transfer rate reduces toward the edges where the local Nusselt number converges to approach 0 (Fig. 10). However, similar to that observed for velocity and temperature profiles the effect of side wall inclination angle  $\phi$  on local Nusselt number is seen to be much stronger in the vicinity of the sloping walls.

On the other hand, it can be observed that as  $Ra$  increases, the magnitude of the local Nusselt number enhances notably and its distribution becomes more non-linear due to the stronger convection effects. In other

words, the gradient of temperature on the hot and cold walls augments with the rise of  $Ra$  and hence increases the local heat transfer. Results show that the maximum of the local heat transfer and nonlinearity of its distribution decrease as  $Y$  increases due to viscous effects. In the case of yield stress fluids, sinusoidally varying Nusselt distribution can be observed in the zone of the upper stagnation point which can be interpreted as a decrease in temperature gradients of upper stagnation point due to the plug region.

#### 4.4. Mean heat transfer

Figs. 11–14 show the effect of the side wall inclination angle ( $\phi = 0, \pi/6, \pi/4, \pi/3$ ) on the mean Nusselt number for different values of yield number ( $0 \leq Y \leq Y_c$ ) at Rayleigh numbers  $Ra = 5.10^3 - 10^5$ , respectively. Based on the previous discussions, the side wall inclination angle ( $\phi$ ) is predicted to have significant effects on the behavior of the average Nusselt number which increases as the side wall inclination angle increases. In other words, the increase in  $\phi$  strengthens the intensity of convection. Here it is observed that the average Nusselt number may increase by 90% as  $\phi$  increases from 0 to  $\pi/3$ . On the other hand, it is seen that the average Nusselt number may increase to more than 100% as  $Ra$  increases from  $5.10^3$  to  $10^5$ .

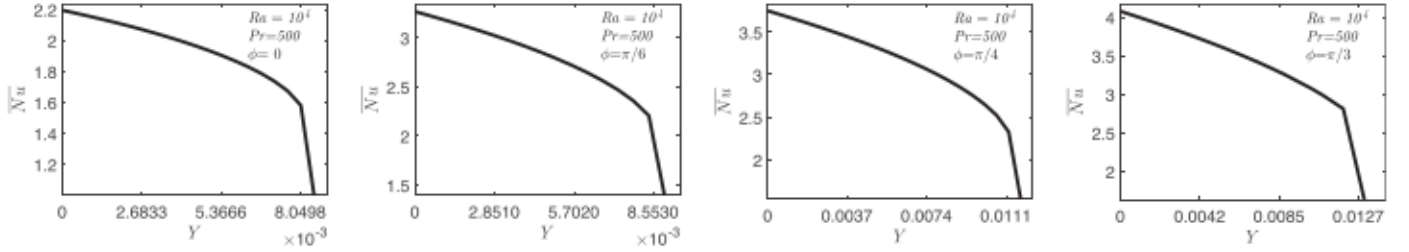


Fig. 12. Variations of mean Nusselt number  $\overline{Nu}$  with yield number  $Y$  along the hot bottom wall for different values of sidewall inclination angle ( $\phi = 0, \pi/6, \pi/4, \pi/3$ ) at  $Ra = 10^4$ .

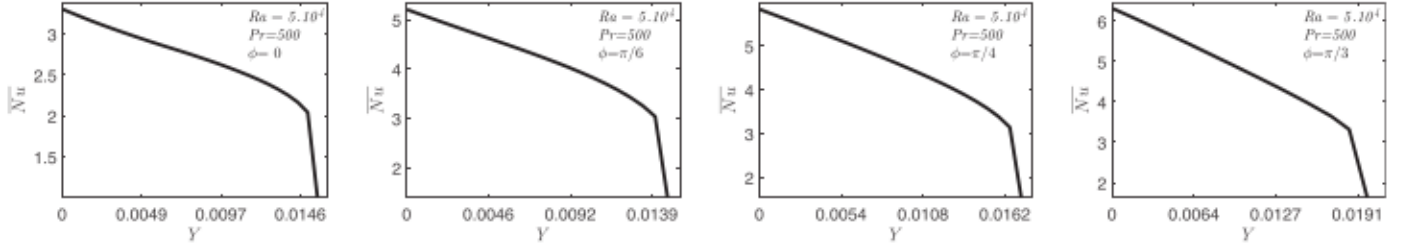


Fig. 13. Variations of mean Nusselt number  $\overline{Nu}$  with yield number  $Y$  along the hot bottom wall for different values of sidewall inclination angle ( $\phi = 0, \pi/6, \pi/4, \pi/3$ ) at  $Ra = 5.10^4$ .

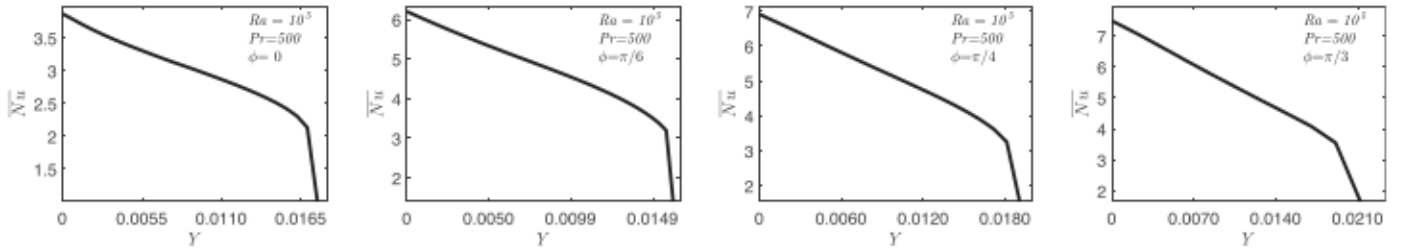


Fig. 14. Variations of mean Nusselt number  $\overline{Nu}$  with yield number  $Y$  along the hot bottom wall for different values of sidewall inclination angle ( $\phi = 0, \pi/6, \pi/4, \pi/3$ ) at  $Ra = 10^5$ .

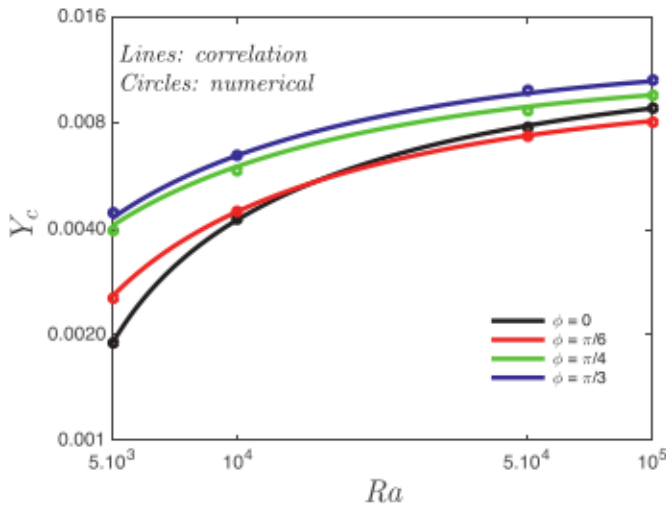


Fig. 15. The variations of critical yield number  $Y_c$  with Rayleigh number  $Ra$  for different values of sidewall inclination angle ( $\phi = 0, \pi/6, \pi/4, \pi/3$ ).

Results show that the heat transfer is maximal for Newtonian fluids ( $Y = 0$ ). But, the increase in yield number leads to reduce the heat transfer since  $\overline{Nu}$  decreases with increasing  $Y$ . Furthermore, whatever the value of  $\phi$  and  $Ra$ , convection finally stops at sufficiently large yield number ( $Y = Y_c$ ) and the heat transfer corresponds only to a conductive

regime ( $\overline{Nu} = \overline{Nu}_c$ ). This is due to the fact that the plug region invades the whole space leading finally to a motionless state. It is observed that, interestingly, the increasing trend of  $Y_c$  (with increasing  $Ra$ ) is more pronounced in square cavity. As a result, at high Rayleigh numbers, the critical yield number  $Y_c$  of square cavity ( $\phi = 0$ ) is larger than that with  $\phi = \pi/6$ . This trend is more clearly shown in Fig. 15. This is due to the fact that, as mentioned earlier, in trapezoidal cavities the plug regions increase as Rayleigh number increases and, as a consequence, affect the critical yield number  $Y_c$ .

A correlation for the critical yield number  $Y_c$  can be estimated by fitting our numerical results as follows:

$$Y_c = (a \cdot \ln(Ra) - b) Ra^{-0.16} \quad (11)$$

$$a = 0.005565 \exp(-4.417\phi) + 0.01048 \exp(0.4314\phi)$$

$$b = 0.08935 \exp(-1.439\phi) + 0.0399 \exp(0.916\phi)$$

This correlation leads to a mean relative difference with our numerical results which is less than 2% for  $5.10^3 \leq Ra \leq 10^5$  and  $0 \leq \phi \leq \pi/3$  as depicted in Fig. 15.

## 5. Conclusions

The objective of this work was to analyze the phenomena of natural convection in a trapezoidal enclosure filled with a yield stress fluid obeying the Bingham model. For this purpose, a finite element numerical code based on the unstructured triangular grid has been developed. The bottom wall is heated and the top wall is cooled isothermally while the sloping walls are considered adiabatic.



Various inclination angles of the sloping wall ( $\varphi = 0, \pi/6, \pi/4, \pi/3$ ), yield numbers ( $0 \leq Y \leq Y_c$ ), and Rayleigh numbers ( $5.10^3 \leq Ra \leq 10^5$ ) have been considered and the flow and temperature fields as well as the heat transfer rate have been investigated. It is found that when the Inclination angle was increased from  $\varphi = 0$  it causes a multicellular flow, which appears as the main parameter to govern heat transfer in the cavity. Results obtained generally show spectacular heat transfer enhancement capabilities when compared to the square cavity ( $\varphi = 0$ ). On the other hand, the results reveal that, the mean heat transfer rate increases with increasing  $Ra$  due to stronger convection effects and decreases with increasing yield number ( $Y$ ) because of strengthening viscous forces.

Contrary to what is expected, it is found that the unyielded regions increase with increasing  $\varphi$  despite the fact that the convective thermal transport strengthens. On the other hand, results show that increasing the yield stress ( $Y$ ) is also accompanied by the increase in the plug regions, reducing the convection intensity in all cases. Above a certain value of  $Y$ , the convection does not occur, and the heat transfer is only due to conduction. Results show that the values of critical yield number ( $Y_c$ ) depend on  $\varphi$  and generally increase with increasing  $\varphi$  due to stronger convection effects. Finally, it is of interest to note here that in trapezoidal enclosure ( $\varphi > 0$ ) the plug regions may increase with increase in  $Ra$  while in square enclosure ( $\varphi = 0$ ) the plug regions always decrease when  $Ra$  is increased.

#### Declaration of Competing Interest

None.

#### CRediT authorship contribution statement

**M.S. Aghighi:** Supervision, Conceptualization, Methodology, Software, Writing - original draft. **A. Ammar:** Supervision, Conceptualization, Writing - review & editing. **H. Masoumi:** Data curation, Visualization, Investigation. **A. Lanjani:** Software, Validation.

#### References

- [1] Bodenschatz E, Pesch W, Ahlers G. Recent developments in Rayleigh-Bénard convection. *Annu Rev Fluid Mech* 2000;32:709–78.
- [2] Ouertatani N, Ben Cheikh N, Ben Beya B, Lili T. Numerical simulation of two-dimensional Rayleigh-Bénard convection in an enclosure. *Comptes Rendus Mécanique* 2008;336(5):464–70.
- [3] Maystrenko A, Resagk C, Thess A. Structure of the thermal boundary layer for turbulent Rayleigh-Bénard convection of air in a long rectangular enclosure. *Phys Rev E* 2007;75(6):066303.
- [4] Tyvand PA. Onset of Rayleigh-Bénard Convection in Porous Bodies. *Transp Phenom Porous Media II* 2002:82–112.
- [5] Aghighi MS, Ammar A, Metivier C, Normandin M, Chinesta F. Non-incremental transient solution of the Rayleigh-Bénard convection model by using the PGD. *J Non-newton Fluid Mech* 2013;200(Oct.):65–78.
- [6] Aghighi S, Ammar A, Metivier C, Chinesta F. Parametric solution of the Rayleigh-Bénard convection model by using the PGD. *Int J Numer Methods Heat Fluid Flow* 2015;25(6):1252–81.
- [7] Park HM. Rayleigh-Bénard convection of nanofluids based on the pseudo-single-phase continuum model. *Int J Therm Sci* 2015;90:267–78.
- [8] Siddheshwar PG, Kanchana C. Unicellular unsteady Rayleigh-Bénard convection in Newtonian liquids and Newtonian nanofluids occupying enclosures : new findings. *Int J Mech Sci* 2017;131–132(Oct.):1061–72.
- [9] Zhang J, Vola D, Frigaard IA. Yield stress effects on Rayleigh-Bénard convection. *J Fluid Mech* 2006;566(Oct.):389–419.
- [10] Vikhansky A. On the onset of natural convection of Bingham liquid in rectangular enclosures. *J Nonnewton Fluid Mech* 2010;165(23–24):1713–16.
- [11] Turan O, Chakraborty N, Poole RJ. Laminar Rayleigh-Bénard convection of yield stress fluids in a square enclosure. *J Nonnewton Fluid Mech* 2012;171–172(Mar.):83–96.
- [12] Hassan MA, Pathak M, Khan MK. Rayleigh-Bénard convection in Herschel-Bulkley fluid. *J Nonnewton Fluid Mech* 2015;226:32–45.
- [13] Aghighi MS, Ammar A. Aspect ratio effects in Rayleigh-Bénard convection of Herschel-Bulkley fluids. *Eng Comput* 2017;34(5):1658–76.
- [14] Aghighi MS, Ammar A, Metivier C, Gharagozlu M. Rayleigh-Bénard convection of Casson fluids. *Int J Therm Sci* 2018;127(May):79–90.
- [15] Nirmalkar N, Bose A, Chhabra RPP. Free convection from a heated circular cylinder in Bingham plastic fluids. *Int J Therm Sci* 2014;83(Sep.):33–44.
- [16] Li C, Magnin A, Métivier C. Natural convection in shear-thinning yield stress fluids in a square enclosure. *AIChE J* 2016;62(4):1347–55.
- [17] Raffei B, Masoumi H, Aghighi MS, Ammar A. Effects of complex boundary conditions on natural convection of a viscoplastic fluid. *Int J Numer Methods Heat Fluid Flow* 2019;29(8):2792–808.
- [18] Masoumi H, Aghighi MS, Ammar A, Nourbakhsh A. Laminar natural convection of yield stress fluids in annular spaces between concentric cylinders. *Int J Heat Mass Transf* 2019;138:1188–98.
- [19] Lee TS. Computational and experimental studies of convective fluid motion and heat transfer in inclined non-rectangular enclosures. *Int J Heat Fluid Flow* 1984;5(1):29–36.
- [20] Karyakin YE. Transient natural convection in prismatic enclosures of arbitrary cross-section. *Int J Heat Mass Transf* 1989;32(6):1095–103.
- [21] Basak T, Roy S, Pop I. Heat flow analysis for natural convection within trapezoidal enclosures based on heatline concept. *Int. J. Heat Mass Transf.* 2009;52(11–12):2471–83.
- [22] Varol Y, Oztop HF, Pop I. Numerical analysis of natural convection in an inclined trapezoidal enclosure filled with a porous medium. *Int J Therm Sci* 2008;47(10):1316–31.
- [23] Saleh H, Roslan R, Hashim I. Natural convection heat transfer in a nanofluid-filled trapezoidal enclosure. *Int J Heat Mass Transf* 2011;54(1–3):194–201.
- [24] Al-Weheibi SM, Rahman MM, Alam MS, Vajravelu K. Numerical simulation of natural convection heat transfer in a trapezoidal enclosure filled with nanoparticles. *Int J Mech Sci* 2017;131–132:599–612.
- [25] Gibanov NS, Sheremet MA, Pop I. Free convection in a trapezoidal cavity filled with a micropolar fluid. *Int J Heat Mass Transf* 2016;99:831–8.
- [26] Miroshnichenko IV, Sheremet MA, Pop I. Natural convection in a trapezoidal cavity filled with a micropolar fluid under the effect of a local heat source. *Int J Mech Sci* 2017;120(Jan.):182–9.
- [27] Hossain MS, Alim MA. MHD free convection within trapezoidal cavity with non-uniformly heated bottom wall. *Int J Heat Mass Transf* 2014;69:327–36.
- [28] Astanina MS, Sheremet MA, Oztop HF, Abu-Hamdeh N. MHD natural convection and entropy generation of ferrofluid in an open trapezoidal cavity partially filled with a porous medium. *Int J Mech Sci* 2018;136:493–502.
- [29] Al-Sayegh R. Influence of external magnetic field inclination on three-dimensional buoyancy-driven convection in an open trapezoidal cavity filled with CNT-Water nanofluid. *Int J Mech Sci* 2018;148(Nov.):756–65.
- [30] Alsabery AI, Chamkha AJ, Saleh H, Hashim I. Transient natural convective heat transfer in a trapezoidal cavity filled with non-Newtonian nanofluid with sinusoidal boundary conditions on both sidewalls. *Powder Technol* 2017;308:214–34.
- [31] Al-Mudhaf AF, Rashad AM, Ahmed SE, Chamkha AJ, EL-Kabeir SMM. Soret and Dufour effects on unsteady double diffusive natural convection in porous trapezoidal enclosures. *Int J Mech Sci* 2018;140(May):172–8.
- [32] Papanastasiou TC. Flows of Materials with Yield. *J Rheol (NYN Y)* 1987;31(5):385–404.
- [33] Dhett G, Touzot G, Lefrançois E. Finite element method. Hoboken, NJ, USA: John Wiley & Sons, Inc.; 2012.
- [34] Mitsoulis E. Flows of viscoplastic materials: models and computations. *Rheol Rev* 2007;2007:135–78.